PHYSICAL REVIEW C VOLUME 42, NUMBER 6 DECEMBER 1990

Transition strengths and deformation in ^{77}Kr

T. D. Johnson, J. W. Holcomb, P. C. Womble, P. D. Cottle, and S. L. Tabor
Department of Physics, Florida State University, Tallahassee, Florida 32306

F. E. Durham and S. G. Buccino
Department of Physics, Tulane University, New Orleans, Louisiana 70118

M. Matsuzaki
Institute of Physics, University of Tsukuba, Ibaraki 305, Japan
(Received 30 July 1990)

High spin states in ^{77}Kr were populated using the ^{48}Ti(^{32}S,2pn)^{77}Kr reaction with a 106 MeV ^{32}S beam from the Florida State University Tandem-LINAC accelerator. Three Compton-suppressed Ge detectors at 95° and one at 18° were used to determine γ-γ coincidence relations, directional correlation ratios and Doppler-shift attenuation lifetimes. The level scheme for the positive-parity band agrees with previous studies up to spin $\frac{37}{2}^+$. New levels at 9913 keV ($\frac{41}{2}^+$) and 11 760 keV ($\frac{45}{2}^+$) have been identified. The negative-parity band was extended to a probable spin state of $\frac{27}{2}^-$, with three new levels identified. The kinematic and dynamic moments of inertia in the positive-parity band converge to a rather constant value of (22–24) $\hbar^2$/MeV. The transition quadrupole moments average about 2.6 e b in this band and decrease somewhat after the $\pi g_{9/2}$ alignment. The magnetic transition strengths alternate with signature and increase to about a nuclear magneton after the alignment. The kinematic moment of inertia in the negative-parity band increases with rotational frequency and exhibits the beginnings of a band crossing at $\hbar\omega \approx 0.55$ MeV, while the transition quadrupole moments decrease steadily with frequency. Cranking model calculations with the Nilsson plus BCS potential were performed for the quasiparticle energies and electromagnetic transition rates for both the positive- and negative-parity bands. The experimental data were reproduced well. As for the positive-parity band, $\beta(3\text{qp}) > \beta(1\text{qp})$ has been shown to be necessary in addition to $\gamma(3\text{qp}) > 0$ to reproduce the signature dependence of the energies and $B(M1)$ values.

I. INTRODUCTION

The light neutron-deficient krypton isotopes form a rich testing ground for nuclear collective models because they can exhibit large quadrupole deformation, and yet their rather soft shapes are strongly influenced by the polarizing effects of quasiparticles and rotation. Deformations as high as $\beta_2 \geq 0.4$ have been reported[1] for ^{74}Kr, while the effects of coexisting weakly deformed low-spin states have been seen[1–3] in all the light, even isotopes ^{72,74,76,78}Kr. The odd Kr isotopes provide an opportunity to clarify the role of quasiparticle alignments through Pauli blocking and to investigate the deformation driving effects of different quasiparticle orbits. Magnetic transitions in the odd isotopes provide valuable information about the triaxial degree of freedom γ and the interaction between deformation- and rotation-aligned quasiparticles.

The nucleus ^{77}Kr is well situated between two of the best known isotopes ^{76}Kr and ^{78}Kr, and understanding of the structure of these nuclei is strongly coupled. For example, an earlier study[4] of quasiparticle alignment in ^{77}Kr led to a better understanding of the known alignments in ^{76}Kr and ^{78}Kr and to a prediction of a higher second crossing in ^{78}Kr. Recent work[5,6] has significantly expanded the level schemes of ^{76,78}Kr, located the predicted second crossing in ^{78}Kr, and invited further exploration of ^{77}Kr. The last study[4] of ^{77}Kr left a number of questions. Uncertainties remained about a possible second band crossing in the positive-parity yrast band, and no information was available about alignments in the negative-parity band. Lifetimes were not known at or above the first $\pi = +$ band crossing to elucidate possible shape changes.

Because so many strong magnetic dipole transitions are known in ^{77}Kr, they allow an excellent opportunity for studying interesting facets of their behavior. An earlier study[4] had demonstrated an alternating pattern of $B(M1)$ strengths which can be related to the signature splitting of the Routhians.[7–10] There were also indications of an increase in magnetic transition strengths after alignment. This was expected semiclassically because of a constructive addition of the magnetic moments of the three quasiparticles. Again, more lifetime information was needed along with more specific calculations to better understand the $B(M1)$ behavior and its relation to quasiparticle moments and triaxially.

Two earlier studies[11,12] of high-spin states in ^{77}Kr established two rotational bands, one built on the $\frac{5}{2}^+$ ground state and another based on the $\frac{3}{2}^-$ state at 66.5 keV. The former was investigated up to a spin of ($\frac{25}{2}^+$) and the latter up to ($\frac{21}{2}^-$). Mean lifetimes and branching and mixing ratios were measured[12] for most of these lev-

els. The results were compared with a triaxial rotor plus quasiparticle model. More recently, Gross *et al.* explored[4] the positive-parity band in ^{77}Kr up to a spin of $(\frac{41}{2}^+)$ and compared the quasiparticle alignments with those in ^{76,78}Kr. Hartree-Fock-Bogolyubov cranking calculations were performed to predict the evolution of shape with rotation and alignment. The alternating pattern of $B(M1)$ strengths was discussed in the context of the semiclassical model[9,13] of Dönau.

The present study of ^{77}Kr was initiated to measure the lifetimes of higher-lying states and to extend knowledge of the negative-parity band up through the band-crossing region. A ^{32}S beam was used to bring more angular momentum into the system than in previous studies, and significantly more events were observed.

II. EXPERIMENTAL PROCEDURE

The reaction used was ^{48}Ti(^{32}S,$2pn$)^{77}Kr. The Florida State University Tandem-LINAC facility was used to produce the ^{32}S beam, which was stripped to an 8^+ charge state in the Tandem and then was injected at 70 MeV into the LINAC and boosted to 106 MeV. A natural Ti target of thickness 0.05 g/cm^2 was used.

The γ-γ coincidence data were collected using four high-purity Compton-suppressed Ge detectors. Three detectors were placed at 95°, and one was at 18° to facilitate lifetime measurements and the extraction of correlation ratios. Over 6×10^8 coincidence events were recorded. To eliminate backscatter, the three 95° detectors were positioned so that no pair was 180° apart in the azimuthal ϕ angle. The resolution of these detectors for the 1332-keV ^{60}Co transition was about 2 keV. After an initial calibration with a ^{152}Eu source, internal calibrations were made based on the following lines: 179.1 keV (^{77}Kr), 300.2 keV (^{77}Kr), 423.9 keV (^{76}Kr), 511.0 keV (e^+e^- annihilation peak), 634.8 keV (^{74}Se), 983.5 keV (from the Coulomb excitation of ^{48}Ti), 1227.0 keV (^{42}Ca), and 1525.0 keV (^{42}Ca). The calibrations were monitored during the course of the experiment and used to gainshift the data when sorting into coincidence arrays.

Coincidence spectra were obtained with the desired energy gates from the coincidence arrays. Background was approximately removed by subtracting an appropriate fraction of the total coincidence spectrum from each projected spectrum.

III. EXPERIMENTAL RESULTS

A. Extension of the positive-parity band

The level scheme deduced from this experiment is shown in Fig. 1. The level scheme for the positive-parity band agrees with previous work[4,11,12] up to spin $\frac{37}{2}^+$ and has been extended up to $\frac{45}{2}^+$ in the favored band.

A sum coincidence spectrum for the positive-parity band is shown in Fig. 2. The new transitions placed in the level scheme are clearly seen along with several other possible transitions which could not be placed with confidence. Seen on the high-energy end of the 1333-keV line is a narrow 1340-keV line. This is probably feeding from a sideband, but coincidence measurements were inconclusive. Coincidence spectra indicate that the $\frac{13}{2}^+$ level is side fed by the narrow 1604-keV transition. This is probably the 1600-keV decay assigned previously as the

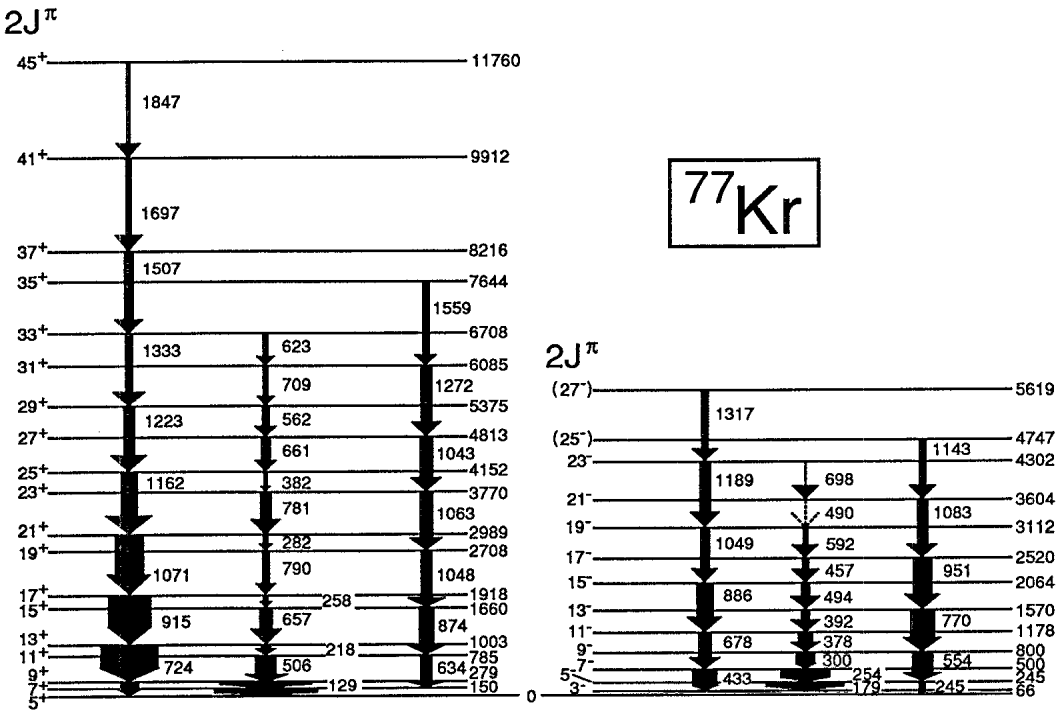

FIG. 1. Energy-level scheme of ^{77}Kr deduced from the present work and previous studies. The 66-keV $\frac{3}{2}^- \rightarrow \frac{5}{2}^+$ transition is not shown for lack of room.

$\frac{41}{2}^+ \rightarrow \frac{37}{2}^+$ transition. However, gates based on higher-lying decays in the current experiment do not support that assignment. The new transitions seen are the 1697- and 1847-keV lines. Individual coincidence spectra based on higher-level decays indicate that both transitions belong in the $\alpha = +\frac{1}{2}$ band. Relative intensity measurements indicate that the 1847-keV transition lies above the 1697-keV decay. Also seen in Fig. 2 is a peak at 1665 keV. Individual coincidence spectra suggest that this transition belongs to the $\pi = +$ band of ^{77}Kr. Unfortunately, gates based on higher-lying levels had too few statistics to establish a placement with any confidence.

Whenever possible, directional correlation of oriented (DCO) nuclei ratios were calculated. The DCO ratio is measured from spectra gated on $E2$ transitions and is given by the ratio of intensity in the 18° spectrum, gated by the 95° line, to the intensity in the 95° spectrum, gated by the 18° line. For states with high angular momentum in this mass region, a DCO ratio of ≈ 1 implies a stretched quadrupole transition and a value of ≤ 0.5 implies a $\Delta J = 1$ transition. This gives a basis with which to assign spins.

The DCO ratios measured for the positive-parity band are summarized in Table I. Gate transitions were based on the 724-, 915-, 1072-, 1163-, 1223-, or 874-keV lines or various combinations of them. The DCO measurement for the 1333-keV transition presented some difficulties due to the 1340-keV line and resulted in somewhat larger error bars. Measurement of the DCO ratios for the 1043- and 1048-keV decays was difficult because of overlapping of these lines with each other and with the 1072- and 1063-keV lines. Gates in which one or more of the overlapping lines were eliminated had relatively poor statistics. In fact, a DCO ratio measurement could not be obtained for the 1063-keV decay. DCO ratio measurements of the 874- and 634-keV transitions have larger uncertainties due to the nearby 634- and 868-keV lines in ^{74}Se. However, the spin assignments for the states deexcited by these transitions have been well established in Refs. 4 and 12. All other DCO ratio measurements confirm the spin assignments of previous studies and indicate the spin assignments for the new 9913- and 11 760-keV levels.

The branching ratios are also shown in Table I. So that all possible decay paths were accounted for, the relative intensities were taken from the 150- and 279-keV gates combined. The results are in general agreement with previous studies[4,12] except for the $\frac{27}{2}^+$, $\frac{23}{2}^+$, and $\frac{19}{2}^+$ decays. In this energy region the different transitions are not well resolved, presenting difficulty in obtaining intensity measurements. However, this difficulty was also present in Ref. 4, and so the present branching ratios were used for subsequent calculations to be discussed in Sec. IV.

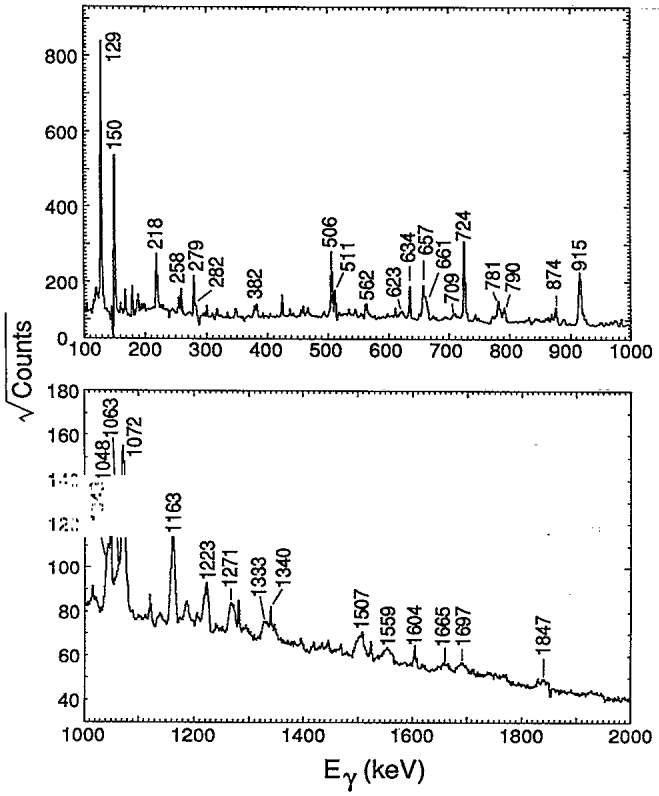

FIG. 2. Sum coincidence spectrum from the positive-parity band based on the addition of 95° spectra gated on the 279-, 724-, 915-, 1072-, 1163-, 1223-, 1332-, 1507-, 150-, 874-, 1048-, 1271-, and 1559-keV lines.

B. Extension of the negative-parity band

A sum of coincidence spectra for the negative-parity band is shown in Fig. 3. All the previously known levels and several new lines are seen clearly. The current results agree with previous work[11,12] on the negative-parity band up to spin $\frac{21}{2}^-$ and an extension is proposed up to $\frac{27}{2}^-$. Included in this level scheme is a 698-keV $\frac{23}{2}^- \rightarrow \frac{21}{2}^-$ transition, and tentatively placed is a 490-keV $\Delta J = 1$ transition linking the $\frac{21}{2}^-$ and $\frac{19}{2}^-$ states. This gives confidence in the placement of the 1189-keV transition. Figure 4 shows two combinations of coincidence gates which indicate the proposed placement of new levels. Weak peaks from transitions of opposite signature can also be observed due to the $\Delta J = 1$ decays. The 1365-keV line seen in Fig. 3 appears to be in the $\pi = -$ band of ^{77}Kr. However, spectra based on gates of the higher transitions gave no clear indication of the placement due to limited statistics. Two additional transitions not shown in the level scheme are seen in the negative-parity sum spectrum in Fig. 3. Gated spectra indicate that the 1121-keV transition feeds the $\frac{19}{2}^-$ level and the $\frac{17}{2}^-$ state is fed by a 1160-keV decay.

Branching ratios for the negative-parity band are shown in Table II. Spectra from gates based on the 66- and 179-keV lines were combined to measure relative populations. Our results are consistent with those of Ref. 12.

The DCO ratios are also summarized in Table II. Gates used to establish DCO ratios were based on the 554-, 770-, 952-, 433-, 678-, 886-, or 1049-keV lines, and on various combinations of them. The 1143- and 1317-keV transitions were indistinguishable from a relatively high background in the forward spectra, and so DCO ra-

tios could not be obtained for these new transitions. The systematics of rotational bands in this mass region suggest that these are $\Delta J=2$ decays. DCO ratios of previously known transitions confirm the earlier spin assignments and give a spin assignment of $\frac{23}{2}^-$ for the 4302-keV level.

C. Lifetime measurements

Lifetimes were measured using the Doppler-shift attenuation method (DSAM) in the 18° coincidence spectra. The Ti target was thick enough to serve as the stopping medium for the recoiling ^{77}Kr nuclei. The decay of the nucleus as it traversed the stopping medium was stimulated by the FIT 1 code developed by E. F. Moore. Discussion of this code is included in Ref. 14 and will not be repeated here. Electronic stopping power values were interpolated from the tabulated values of Northcliffe and Schilling.[15] Nuclear stopping powers were calculated using Bohr's ansatz.[16,17] Angular straggling at low recoil velocities due to atomic collisions was treated using Blaugrund's approximation.[18] The distribution of recoil velocities of the ^{77}Kr nuclei was assumed to be Gaussian.[19]

Lifetimes were fitted systematically starting with the highest levels, and these were used for feeding corrections working down the cascade. Side-feeding lifetimes are also needed for feeding corrections. The side-feeding time for the $\frac{37}{2}^+$ state was taken to be 0.05 ps and was assumed to increase by 0.03 ps per level of deexcitation, consistent with previous studies.[1,12,14,20] The side-feeding time for the $\frac{27}{2}^-$ state was assumed to be 0.1 ps with an increment of 0.03 ps per level also.

Theoretical line shapes were calculated using the lifetime of the state of interest as the variable parameter and were compared with the experimental data using a reduced χ^2 to indicate a goodness of fit. The lifetime chosen for our measured value was that which minimized the reduced χ^2.

Sample lifetime fits are shown in Fig. 5, and all lifetimes are summarized in Table III. Previous measurements are also shown for comparison. It was possible to extend lifetime measurements up to $\frac{37}{2}^+$ for the favored band and up to $\frac{31}{2}^+$ in the unfavored band. In all cases where a DSAM analysis could be performed, our present results were taken as the adopted lifetimes. Overlapping

TABLE I. Intensities, branching ratios, and DCO ratios for the positive-parity band in ^{77}Kr.

E_x (keV)	E_γ (keV)	I_γ	Branching ratio (%)	Branching[a] ratio (%)	Branching[b] ratio (%)	R_{DCO}
150.4	150.4	181(18)				0.29(1)
279.1	279.1	27(5)	13(2)		12(2)	0.83(4)
	128.8	180(14)	87(2)		88(2)	0.31(1)
784.8	634.5	15(1)	30(2)	25(3)	28(3)	0.86(20)
	505.6	35(2)	70(2)	75(3)	72(3)	0.28(5)
1003.3	724.1	100	86(2)	82(2)	94(3)	1.14(6)
	218.6	17(2)	14(2)	18(2)	6(3)	0.44(3)
1659.7	874.8	24(2)	52(2)	52(4)	63(5)	0.70(20)
	657	22(1)	48(2)	48(4)	37(5)	0.16(10)
1918.0	914.7	80(4)	93(1)	96(1)	98(1)	1.09(5)
	258.3	6(1)	7(1)	4(1)	2(1)	0.44(3)
2707.6	1048	9(2)	41(6)	63(3)		
	789.7	13(2)	59(6)	37(3)		0.59(9)
2989.3	1071.4	54(4)	95(2)	>91	>94	0.90(11)
	282	3(1)	5(2)	<9	<9	0.32(17)
3770.1	1063.0	18(4)	51(6)	39(3)		
	780.2	17(2)	49(6)	61(3)		0.33(8)
4152.1	1162.4	33(1)	92(3)	84(2)	>65	1.12(5)
	382.4	3(1)	8(3)	16(2)	<35	0.32(9)
4813.2	1043.1	21(13)	70(13)	33(3)		0.69(22)
	661	9(1)	30(13)	67(3)		0.46(9)
5375.3	1223.2	14(4)	67(6)	63(3)		1.05(14)
	562	7(4)	33(6)	37(3)		0.35(14)
6084.9	1271.7	16(2)	80(8)	>63		1.05(17)
	709	4(2)	20(8)	<37		
6708.3	1333.0	11.0(1.9)	65(3)	>50		0.87(27)
	623	6(3)	35(3)	<50		
7644	1559	9(4)				0.90(20)
8215.7	1507.4	11.3(4.0)				1.02(15)
9912.4	1696.7	8(3)				0.97(24)
11 759.5	1847.1	5(2)				1.09(28)

[a]Reference 4.

[b]Reference 12.

TABLE II. Intensities, branching ratios, and DCO ratios for the negative-parity band in ^{77}Kr.

E_x (keV)	E_γ (keV)	I_γ	Branching ratio (%)	Branching[a] ratio (%)	R_{DCO}
66.5	66.5	22(11)			
245.3	245.0	10(5)	7(3)		
	179.1	133(7)	93(3)		0.34(1)
499.8	433.4	42(6)	33(3)	21(4)	0.91(4)
	254.4	84(3)	67(3)	79(4)	0.29(1)
799.8	554.4	33(2)	53(2)	53(3)	1.00(4)
	300.2	29(1)	47(2)	47(3)	0.34(2)
1177.6	677.7	26(1)	54(2)	67(3)	1.06(5)
	377.8	22(1)	46(2)	33(3)	0.30(2)
1569.8	769.8	40(1)	74(2)	76(3)	1.01(6)
	392.4	14(1)	26(2)	24(3)	0.38(2)
2063.6	886.0	28(2)	72(2)	77(5)	1.13(8)
	494	11(1)	28(2)	23(5)	0.22(4)
2520.5	950.9	29(2)	83(3)	67(10)	1.03(4)
	456.7	6(1)	17(3)	33(10)	0.43(5)
3112.5	1049.1	14(1)	82(10)		0.92(7)
	592.0	3(2)	18(10)		0.30(10)
3603.8	1083.3	19(2)			0.96(15)
	(490)				
4302.0	1189.5	16(2)	95(2)		0.99(16)
	698	0.8(3)	5(2)		
4747	1143	8(3)			
5619.1	1317.1	11(2)			

[a]Reference 12.

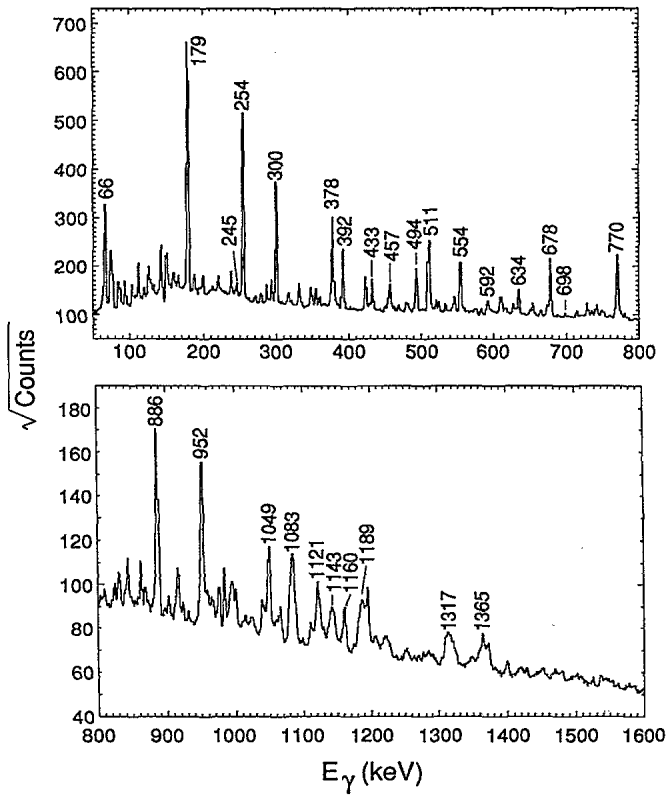

FIG. 3. Sum coincidence spectrum from the negative-parity band based on the addition of 95° spectra gated on the 554-, 770-, 952-, 433-, 678-, 886-, 1049-, 1083-, 179-, 254-, and 300-keV lines.

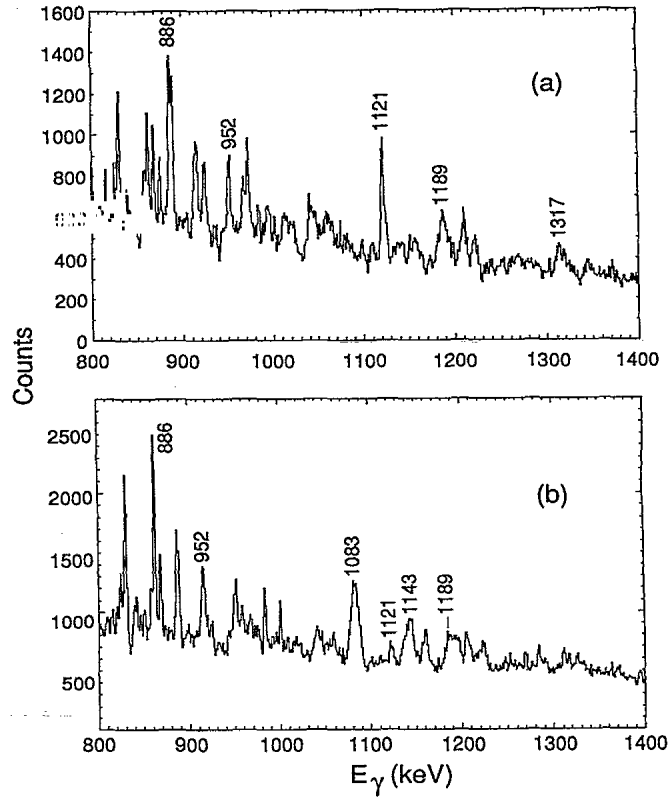

FIG. 4. Portion of the coincidence spectra obtained by the addition of spectra gated on (a) the 1049- and 592-keV transitions, and (b) the 1083-, and 952-keV transitions.

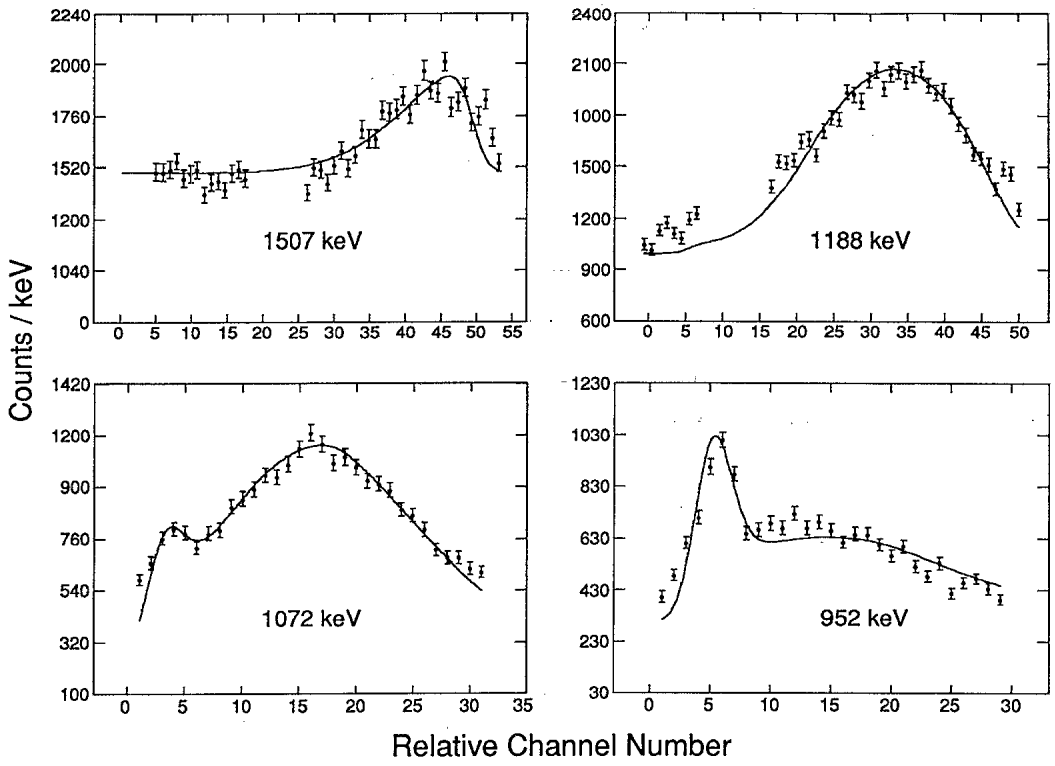

FIG. 5. Doppler-shifted line shapes observed at 18°. The smooth curves are theoretical line shapes fitted to the data, as discussed in the text. The data are taken from coincidence gated spectra.

of the 1043-, 1048-, 1063-, and 1072-keV lines made lifetime measurements difficult in this energy region of the positive-parity band. However, through a judicious choice of transitions on which to base coincidence gates, much of the overlapping was minimized. In the negative-parity band, lifetimes were measured up through the $\frac{27}{2}^-$ state. No value could be obtained for the $\frac{25}{2}^-$ level because of contaminants near the 1143-keV transition.

Lifetimes reported earlier by Wörmann *et al.*[12] are included in Table III for comparison. The values are generally similar, although the present ones tend to be somewhat shorter. In making the comparison one should remember that those lifetimes which could not be corrected for feeding are basically upper limits. In the case of the $\frac{17}{2}^+$ state, the present lifetime of 0.56(11) ps is closer to the previous[12] DSAM value of 0.76(15) ps than to the recoil-distance method determination of 1.0(15) ps made in the same work.

The electromagnetic transition strengths $B(M1)$ and $B(E2)$ calculated from these lifetimes are given in Tables IV and V. Since angular distributions were not measured in this experiment, the mixing ratios δ of Refs. 4 and 12 were used for the $\Delta J=1$ transitions. For the higher transitions where the mixing ratios have not been measured, a value of $\delta=0.10(10)$ was used to calculate $B(M1)$. A small value of δ is consistent with the measured DCO ratios and has little effect on $B(M1)$. On the other hand, no $B(E2)$ values could be calculated for these cases because $B(E2)$ scales with δ^2. The magnitudes of the transition quadrupole moments Q_t were calculated from the rotational model formula

$$Q_t^2=(16\pi/5)<J_iK20|J_fK>^{-2}B(E2;J_i\rightarrow J_f)\ ,$$

and are listed in Tables IV and V. An effective value of $K=\frac{5}{2}$ $(\frac{3}{2})$ was used for the $\pi=+$ $(-)$ bands. For the $\Delta J=2$ transitions, the axial quadrupole deformations β_2, which would give the observed moments, were determined from

$$\beta_2=-(7\sqrt{\pi/80}+(49\pi/80+7\pi Q_t/6eZr_0^2A^{2/3})^{1/2}\ ,$$

with $r_0=1.2$ fm.

IV. DISCUSSION

A. Positive-parity band

It is useful to examine the band structure of ^{77}Kr in terms of the cranking model. It also proves insightful to compare moments of inertia, band crossings, and transition strengths with those of neighboring nuclei.

The kinematic ($J^{(1)}$) and dynamic ($J^{(2)}$) moments of inertia in the positive-parity band in ^{77}Kr are shown in Fig. 6, along with those for the neighboring odd isotopes ^{75}Kr (Refs. 21 and 22) and ^{79}Kr.[23] It is interesting to note that the lowest frequency $\alpha=+\frac{1}{2}$ J^1 values are anomalously high for both ^{75}Kr and ^{77}Kr. A similar effect among the even Kr isotopes has been interpreted[1,3] as arising from shape coexistence.

The quasiparticle alignments differ for the two signa-

tures. For the $\alpha=+\frac{1}{2}$ bands, the alignment frequency increases somewhat with decreasing mass. For ^{77,79}Kr the alignment is sharper for the $\alpha=-\frac{1}{2}$ bands, while not enough is known about ^{75}Kr to determine the $\alpha=-\frac{1}{2}$ band crossing. Overall, the alignment behavior is similar for the three nuclei. The blocking argument indicates that the band crossings are all due to the alignment of a pair of $g_{9/2}$ protons, as discussed in Refs. 4 and 21–23.

After the alignment, the kinematic moment of inertia in the favored signature of ^{77}Kr attains a constant value of $24\hbar^2$/MeV, close to that of the dynamic moment. The kinematic and dynamic moments of inertia also appear to be converging for the unfavored signature. This convergence and stabilization of the moments of inertia of ^{77}Kr occur at about the same frequency and value as was attributed[24] to the onset of rigid rotation in ^{84}Zr. Investigation of a few more levels in ^{75}Kr would establish whether a similar effect occurs there.

The aligned angular momentum can be seen more directly by subtracting out the angular momentum due to collective rotation ($I_x - I_{\text{ref}}$). Establishing I_{ref} is not a simple matter among these nuclei. For the reference angular momentum, we have used the Harris parametrization of Ref. 4 ($J_0=10\hbar^2$/MeV and $J_1=5\hbar^4$/MeV^3). The results for the positive-parity band of ^{77}Kr are graphed in Fig. 7(b) along with those for ^{76}Kr and ^{78}Kr.[5,6] More has been learned about all three nuclei since an earlier version of this graph was presented,[4] but the behavior of the first alignment due to a $g_{9/2}$ proton pair remains unchanged. The predicted $\nu g_{9/2}$ alignment in ^{78}Kr has since been observed[5,6] at $\hbar\omega\approx 0.9$ MeV, showing a similar total gain in aligned angular momentum for both ^{76}Kr and ^{78}Kr. In ^{77}Kr the small change in the position of the $\frac{41}{2}^+$ level and the new $\frac{45}{2}^+$ state have pushed the possible beginning of a second alignment up to $\hbar\omega\approx 0.9$ MeV.

The $\Delta J=2$ transition quadrupole moments are presented as a function of rotational frequency in Fig. 8(a). The $|Q_t|$ values average about 2.6 e b in the one-quasiparticle (qp) band, dip sharply at the alignment (for $\alpha=-\frac{1}{2}$), and may be somewhat lower above it. Hence the yrast configuration of ^{77}Kr with an average $\beta_2\approx 0.33$ is less deformed than that of ^{74}Kr (Ref. 1), but more deformed than those of the heavier odd isotopes[23] as would be expected from the general systematics,[25] which imply a maximum deformation at midshell ($N=39$).

The behavior of the strong magnetic transitions shown in Fig. 8(b) is particularly interesting. There is a large alternation of strengths in the 1-qp band with larger (smaller) $B(M1)$ values for those transitions leaving states of

TABLE III. Current measured lifetimes in ^{77}Kr and comparison with previous values.

E_γ (keV)	J^π	τ (ps)	τ (ps)[a]
66	$\frac{3}{2}^-$		170(17)[b] ns
179	$\frac{5}{2}^-$		54(5)
433	$\frac{7}{2}^-$		7.5(12)
554	$\frac{9}{2}^-$		3.8(4)
678	$\frac{11}{2}^-$	1.54(31)	1.8(2)
770	$\frac{13}{2}^-$	0.87(17)	1.0(2)
886	$\frac{15}{2}^-$	0.84(17)	1.3[c]
951	$\frac{17}{2}^-$	0.51(10)	1.0(2)[c]
1049	$\frac{19}{2}^-$	0.51(10)	
1083	$\frac{21}{2}^-$	0.47(9)[c]	
1189	$\frac{23}{2}^-$	0.11(2)	
1317	$\frac{27}{2}^-$	0.20(4)[c]	
150	$\frac{7}{2}^+$		
279	$\frac{9}{2}^+$		192(10)
634	$\frac{11}{2}^+$	1.71(34)	3.0(5)
724	$\frac{13}{2}^+$	2.59(78)	2.7(3)
874	$\frac{15}{2}^+$	0.74(15)	1.2(2)
915	$\frac{17}{2}^+$	0.56(11)	0.90(15)
1048	$\frac{19}{2}^+$	0.43(13)	0.4(2)[c]
1072	$\frac{21}{2}^+$	0.23(5)	0.26(8)
1063	$\frac{23}{2}^+$	0.30(6)	
1163	$\frac{25}{2}^+$	0.16(3)	0.44(15)[c]
1043	$\frac{27}{2}^+$	0.24(5)	
1223	$\frac{29}{2}^+$	0.23(5)	
1272	$\frac{31}{2}^+$	0.13(3)[c]	
1333	$\frac{33}{2}^+$	0.08(2)	
1507	$\frac{37}{2}^+$	0.09(2)[c]	

[a]Reference 12.
[b]Reference 11.
[c]Not corrected for feeding.

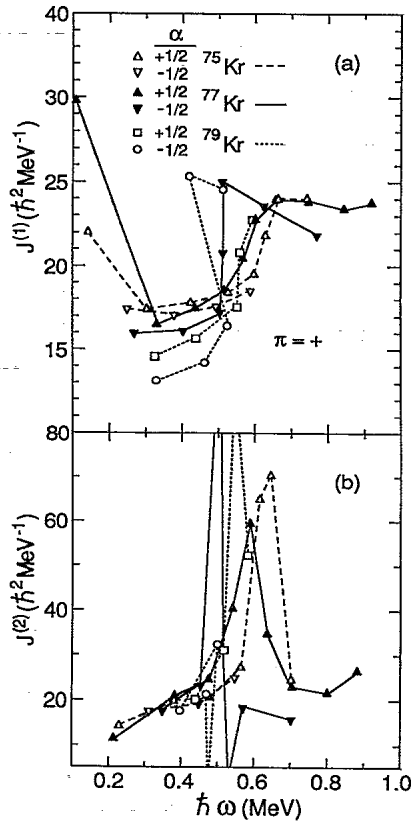

FIG. 6. Plots of the kinematic ($J^{(1)}$) and dynamic ($J^{(2)}$) moments of inertia for the lowest positive-parity bands in ^{77}Kr, ^{75}Kr, and ^{79}Kr.

favored $\alpha=+\frac{1}{2}$ (unfavored $\alpha=-\frac{1}{2}$) signature. This alternation can be related to the signature splitting.[7–10] The signature splitting in the energy levels can be seen from the Routhians in Fig. 7(a) and in an amplified form in Fig. 8(c). It is relatively large in the $\pi=+$ 1-qp band, rising to over 250 keV before the alignment. Above this drop it rises again with increasing frequency in the 3-qp band.

The increase in $B(M1)$ strength after the band crossing may arise from the constructive addition of the $\pi g_{9/2}$ rotation-aligned and $\nu g_{9/2}$ deformation-aligned magnetic moments. A quantitative theoretical discussion of the transition strengths follows in Sec. V. Somewhat similar phenomena have been seen in ^{79}Kr,[23] ^{81}Kr,[26] ^{83}Kr,[27] and ^{81}Sr.[14]

B. Negative-parity band

The kinematic and dynamic moments of inertia for the negative-parity bands of ^{75}Kr (Refs. 21 and 22) and ^{77}Kr are graphed in Fig. 9. The bands might be expected to behave similarly since both have been attributed[9,21,22] to a $\nu[301]\frac{3}{2}$ configuration. A close similarity can be seen in their moments of inertia, with that of ^{75}Kr a little larger. There is evidence for a band crossing just below 0.6 MeV/$\hbar$ for the $\alpha=-\frac{1}{2}$ signature in ^{75}Kr and for the onset of a crossing at 0.55 MeV/$\hbar$ in the $\alpha=+\frac{1}{2}$ signature band of ^{77}Kr. In each case the band of opposite signature shows no sign of an alignment over the observed frequency range, suggesting some signature dependence to the alignment process. Since the $\nu g_{9/2}$ orbitals are not blocked, a neutron alignment is predicted[4] to follow the proton crossing as in ^{76}Kr, but neither nucleus has been investigated to high enough spins to test this.

Another feature of the kinematic moments of inertia is a steady increase with frequency. At first, one might attribute this trend to a steadily increasing deformation, but the transition quadrupole moments for ^{77}Kr in Fig. 10(a) do not support this. Instead, they decrease with increasing rotational frequency, except for one point. Garrett *et al.*[28] have discussed the rotationally induced depopulation of certain quasiparticle orbits which can cause the moment of inertia to increase while the quadrupole moment decreases.

In contrast to the positive-parity band, the $M1$ strengths [Table V and Fig. 10(b)] show almost no signature dependence, a result which is probably due to the lack of signature splitting among the energy levels. The signature splitting of the negative-parity Routhians in Figs. 7(a) and 10(c) is less than 50 keV. Another contrast

TABLE IV. Transition strengths and deformations for the positive-parity rotational band in ^{77}Kr.

E_x (keV)	J	E_γ (keV)	ΔJ	δ	$B(M1)$ (μ_N^2)	$B(E2)$ (W.u.)	$\lvert Q_t\rvert$ (e b)	$\lvert\beta_2\rvert$[a]
279	$\frac{9}{2}$	279	2			21^{+5}_{-3}	$2.01^{+0.24}_{-0.18}$	0.26
		129	1	0.1(1)[b]	$0.12^{+0.01}_{-0.01}$			
785	$\frac{11}{2}$	634	2			72^{+18}_{-12}	$2.88^{+0.34}_{-0.25}$	0.36
		506	1	0.35(6)	$0.16^{+0.03}_{-0.04}$	56^{+23}_{-19}	$2.18^{+0.45}_{-0.37}$	
1003	$\frac{13}{2}$	724	2			70^{+47}_{-20}	$2.52^{+0.74}_{-0.39}$	0.32
		218	1	0.03(5)	$0.30^{+0.07}_{-0.13}$	4^{+12}_{-4}	$0.60^{+0.90}_{-0.60}$	
1660	$\frac{15}{2}$	874	2			58^{+5}_{-10}	$2.14^{+0.26}_{-0.19}$	0.27
		657	1	0.21(5)	$0.12^{+0.02}_{-0.03}$	9^{+5}_{-4}	$1.14^{+0.32}_{-0.25}$	
1918	$\frac{17}{2}$	915	2			110^{+27}_{-18}	$2.82^{+0.33}_{-0.24}$	0.35
		258	1	0.09(7)	$0.41^{+0.07}_{-0.10}$	37^{+78}_{-34}	$2.60^{+2.70}_{-2.00}$	
2708	$\frac{19}{2}$	1048	2			32^{+8}_{-6}	$1.49^{+0.19}_{-0.13}$	0.20
		790	1	0.32(6)	$0.14^{+0.03}_{-0.06}$	17^{+10}_{-7}	$1.91^{+0.56}_{-0.39}$	
2989	$\frac{21}{2}$	1071	2			122^{+34}_{-22}	$2.83^{+0.37}_{-0.27}$	0.35
		282	1	0.1(1)[b]	$0.55^{+0.10}_{-0.15}$			
3770	$\frac{23}{2}$	1063	2			53^{+13}_{-9}	$1.83^{+0.22}_{-0.16}$	0.24
		780	1	0.25(6)	$0.18^{+0.03}_{-0.05}$	14^{+8}_{-6}	$2.04^{+0.58}_{-0.44}$	
4152	$\frac{25}{2}$	1162	2			112^{+26}_{-18}	$2.64^{+0.29}_{-0.18}$	0.33
		382	1	0.07(7)	$0.51^{+0.08}_{-0.12}$	13^{+6}_{-13}	$2.13^{+0.50}_{-2.13}$	
4813	$\frac{27}{2}$	1043	2			98^{+26}_{-17}	$2.44^{+0.30}_{-0.22}$	0.31
		661	1	0.09(5)	$0.24^{+0.04}_{-0.06}$	3^{+5}_{-3}		
5375	$\frac{29}{2}$	1223	2			44^{+12}_{-8}	$1.62^{+0.21}_{-0.15}$	0.21
		562	1	0.00(7)	$0.46^{+0.08}_{-0.13}$	0^{+5}_{-0}		
6085	$\frac{31}{2}$	1272	2			>8	>2.1	>0.27
		709	1		>0.24			
6708	$\frac{33}{2}$	1333	2			81^{+27}_{-16}	$2.17^{+0.34}_{-0.23}$	0.28
		623	1	0.1(1)[b]	$1.02^{+0.20}_{-0.34}$			
8216	$\frac{37}{2}$	1507	2			>60	>1.8	>0.24

[a]Assuming axial symmetry.
[b]Assuming $|\delta|=0.10(10)$.

TABLE V. Transition strengths and deformations for the $K=\frac{3}{2}^-$ rotational band in ^{77}Kr.

E_x (keV)	J	E_γ (keV)	ΔJ	δ	$B(M1)$ (μ_N^2)	$B(E2)$ (W.u.)	$\lvert Q_t\rvert$ (e b)	$\lvert\beta_2\rvert$[a]
245	$\frac{5}{2}$	179	1	0.1[b]	$0.17^{+0.01}_{-0.2}$			
500	$\frac{7}{2}$	433	2			99^{+25}_{-16}	$3.69^{+0.44}_{-0.32}$	0.45
		254	1	0.05(5)[c]	$0.31^{+0.05}_{-0.08}$			
800	$\frac{9}{2}$	554	2			112^{+28}_{-19}	$3.20^{+0.38}_{-0.28}$	0.39
		300	1	0.08(3)	$0.26^{+0.04}_{-0.06}$	14^{+12}_{-8}	$1.38^{+0.60}_{-0.40}$	
1178	$\frac{11}{2}$	678	2			103^{+26}_{-17}	$2.81^{+0.33}_{-0.25}$	0.35
		378	1	0.18(3)	$0.31^{+0.05}_{-0.08}$	51^{+22}_{-18}	$1.46^{+0.31}_{-0.26}$	
1570	$\frac{13}{2}$	770	2			121^{+29}_{-20}	$2.91^{+0.33}_{-0.25}$	0.36
		392	1	0.12(2)	$0.28^{+0.05}_{-0.07}$	19^{+8}_{-6}	$2.29^{+0.48}_{-0.36}$	
2064	$\frac{15}{2}$	886	2			66^{+17}_{-11}	$2.08^{+0.25}_{-0.18}$	0.27
		494	1	0.1[b]	$0.16^{+0.03}_{-0.04}$			
2520	$\frac{17}{2}$	951	2			88^{+22}_{-14}	$2.37^{+0.27}_{-0.20}$	0.30
		457	1	0.1[b]	$0.20^{+0.03}_{-0.05}$			
3112	$\frac{19}{2}$	1049	2			52^{+13}_{-18}	$1.79^{+0.21}_{-0.15}$	0.23
		592	1	0.1[b]	$0.10^{+0.02}_{-0.02}$			
3604	$\frac{21}{2}$	1083	2			>60	>1.9	>0.25
		(490)	1					
4302	$\frac{23}{2}$	1189	2			152^{+34}_{-23}	$3.00^{+0.32}_{-0.24}$	0.37
		698	1	0.1[b]	$0.08^{+0.01}_{-0.02}$			
5619	$\frac{27}{2}$	1317	2			>53	>1.8	>0.23

[a]Assuming axial symmetry.
[b]Assumed $|\delta|=0.10(10)$.
[c]Used $|\delta|=0.05(5)$, Ref. 4.

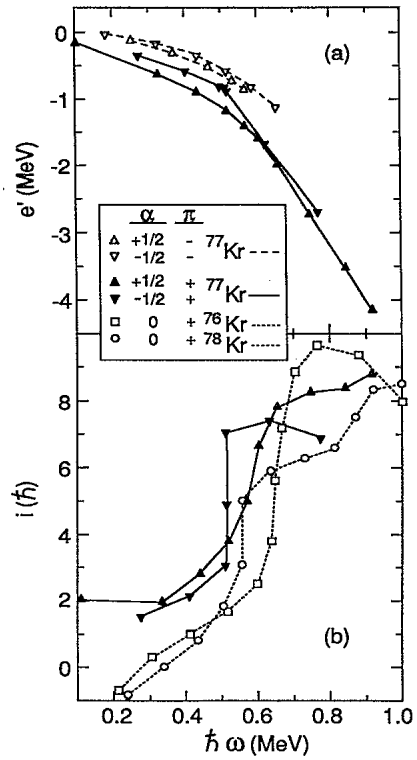

FIG. 7. (a) Routhians e' for the lowest positive- and negative-parity bands in ^{77}Kr. (b) Aligned momenta i for the lowest positive-parity bands in ^{76,77,78}Kr. The Harris parameters used for the reference are $J_0=10\hbar^2/\text{MeV}$ and $J_1=5\hbar^4/\text{MeV}^3$.

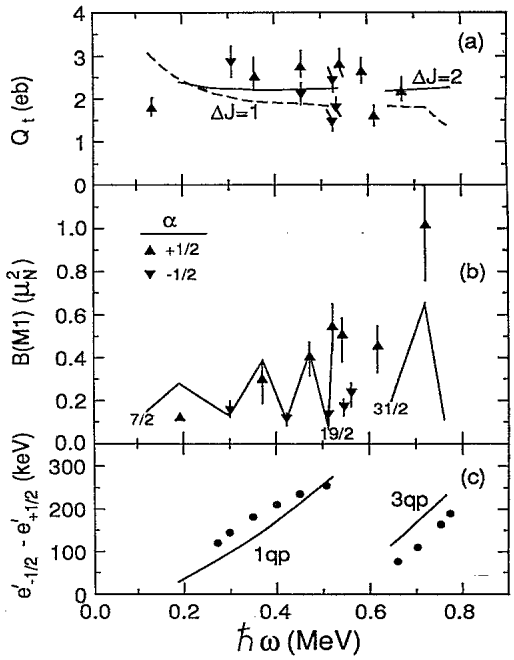

FIG. 8. Comparison of measured and calculated quantities in the positive-parity yrast band of ^{77}Kr. (a) Transition quadrupole moments for the $\Delta J=2$ transitions inferred from the measured lifetimes are shown as points, while the theoretical values for $\Delta J=1$ and 2 are shown as smooth lines. The theoretical Q_t ($\Delta J=2$) values were calculated at the same ω points as those for $\Delta J=1$ transitions for simplicity because Q_t ($\Delta J=2$) varies smoothly with ω. (b) The symbols for the measured $B(M1)$ strengths refer to the signatures of parent states, and the line represents the calculation. (c) The measured (points) and calculated (lines) signature splittings.

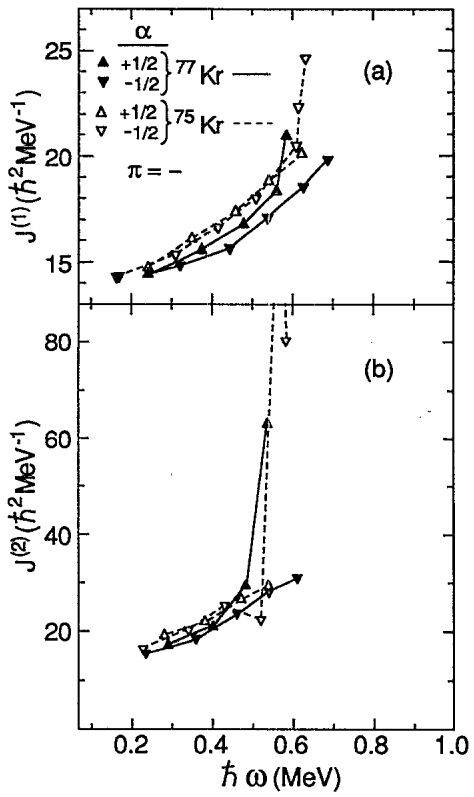

FIG. 9. Kinematic ($J^{(1)}$) and dynamic ($J^{(2)}$) moments of inertia plotted for the negative-parity bands of ^{75}Kr and ^{77}Kr.

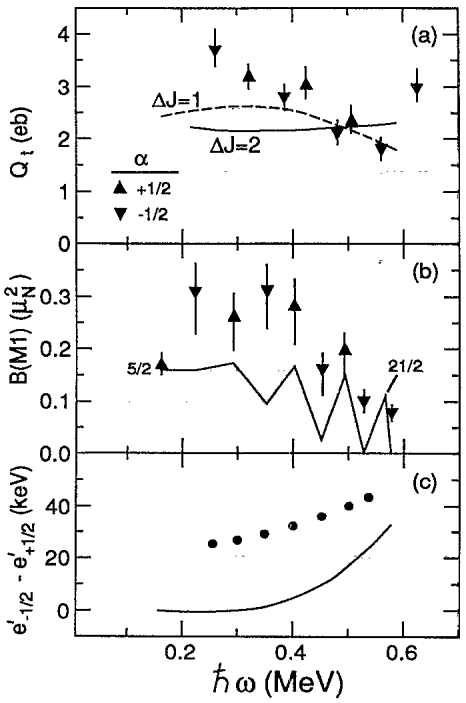

FIG. 10. Comparison of measured and calculated quantities in the negative-parity band of ^{77}Kr. Refer to the caption of Fig. 8 for more information.

is the decrease, rather than increase, in $M1$ strength after the band crossing.

V. THEORETICAL CALCULATION WITH THE NILSSON POTENTIAL

The nuclear shapes in the $A \simeq 80$ region have mainly been discussed in terms of the Woods-Saxon potential. As an alternative approach, we here apply a model[29] based on the Nilsson potential, which has been describing the electromagnetic properties of rare-earth nuclei successfully, to ^{77}Kr. Our calculations were done in a model space consisting of $2 \leq N \leq 4$ both for neutrons and protons, and so we can treat high-j orbitals—the positive-parity intruder shell with $N=4$ in the present case—and low-j orbitals—negative parity, $N=3$—on the same footing without introducing the single-j approximation. Namely, our $M1$ matrix elements are not just multiples of angular momentum matrix elements, and our $B(E2)$ values are calculated using microscopic expectation values of quadrupole moments at each β, γ, and ω. The important effect of the many-j mixing on $M1$ transition rates in low-j natural parity orbitals was discussed in Ref. 10.

Following the prescription given by Matsuzaki, Shimizu, and Matsuyanagi, which is based on the $1/I$ expansion,[29] we adopt their principal-axis (PA) frame operators aside from the vibrational terms:

$$\mu_{-1}^{(\mathrm{PA})} = (g_l - g_R) I_{-1}^{(\mathrm{odd})} + (g_s^{(\mathrm{eff})} - g_R) s_{-1}^{(\mathrm{odd})} ,$$

$$\frac{1}{t} Q_{2-1}^{(\mathrm{PA})} = -\left[\frac{3}{2}\right]^{1/2} \langle Q_0 \rangle \frac{J_z^{(\mathrm{odd})}}{I_0} + \langle Q_2 \rangle \left[2 \frac{i J_y^{(\mathrm{odd})}}{I_0} + \frac{J_z^{(\mathrm{odd})}}{I_0} \right] + \frac{1}{i} Q_{2-1}^{(\mathrm{odd})} , \quad (1)$$

$$Q_{2-2}^{(\mathrm{PA})} = -\left[\frac{3}{8}\right]^{1/2} \langle Q_0 \rangle - \frac{1}{2} \langle Q_2 \rangle + Q_{2-2}^{(\mathrm{odd})} ,$$

where $Q_{2-\Delta J}$ ($\Delta J = 1,2$) are quantized along the rotation axis (x axis), while $\langle Q_k \rangle$ ($K=0,2$) are quantized along the z axis. The quantity I_0 is the angular momentum of the even-even reference state and is assumed to be related to the odd-mass system quantities as

$$I_0 = \langle J_x \rangle = I - i_x , \quad (2)$$

where i_x is the aligned angular momentum of the odd quasiparticle. The notation i_n will be used henceforth because we treat an odd-N nucleus here. Besides, we introduce the geometrical factors referring to Dönau's work[9] in order to improve the description of the low-spin region (see the Appendix of Ref. 30).

Wave functions on which the above operators act were obtained by diagonalizing

$$h' = h_{\mathrm{Nils}} - \Delta(P^\dagger + P) - \lambda N - \hbar\omega J_x . \quad (3)$$

Triaxial deformation can be introduced by $\omega_x \neq \omega_y$ in h_{Nils}. Nilsson parameters $v_{ll} = -0.0268\hbar\omega_0$ for neutrons, $-0.0382\hbar\omega_0$ for protons, and $v_{ls} = -0.127\hbar\omega_0$ both for

neutrons and protons were used with $\hbar\omega_0 = 41A^{-1/3}$ MeV. In the actual diagonalization, the diabatic basis was constructed using the ω expansion[29,31] up to the second order to describe each configuration properly. Therefore, the band-crossing region is omitted in the following calculation.

The effective spin g factor $g_s^{(\text{eff})} = 0.75 g_s^{(\text{free})}$ was used, but no effective charge was introduced. Other parameters are listed in Table VI.

A. [422 $\frac{5}{2}$] 1-qp band

As was done in a previous work on ^{77}Kr,[4] axial symmetry was assumed for simplicity in order to understand the essential nature of this band. Adopting $\beta^{(\text{pot})} = 0.26 (\beta^{(\text{den})} \simeq 0.31)$ (Ref. 32) and $\Delta n = \Delta p = 1.3$ MeV, the pairing force strengths $G_n = 0.0269\hbar\omega_0$ and $G_p = 0.0286\hbar\omega_0$ and the chemical potentials were determined at the ground state ($\omega = 0$) so as to reproduce the correct particle numbers. This mean field reproduces excellently the experimental energy spectra: the signature splittings [Fig. 8(c)] and the alignments, which are associated with the quasineutron orbital, and the first band-crossing frequency $\hbar\omega_c \simeq 0.50$ MeV, which is associated with the lowest quasiproton orbital. We note here that the calculated $\hbar\omega_c$ is common to both signatures in the present calculation.

Further information about the single-quasiparticle state comes from the $M1$ transition between the signature partners. The signature dependence and absolute magnitudes of the $M1$ transitions are reproduced very well using $g_R = 0.3$, as can be seen in Fig. 8(b). However, this value of g_R is smaller than the calculated value of about $Z/A = 0.47$ (g_{RPA} in the notation of Ref. 29). These same calculations have satisfactorily reproduced the experimental values for g_R for many even-even nuclei (see Fig. 1 of Ref. 29 and Fig. 2 of Ref. 10, for example). A similar disagreement between experimental and calculated values of g_R was also reported in Ref. 29 for ^{161}Dy, ^{167}Er, and $^{161-167}$Yb, where the $B(M1)$ strengths were reproduced with $g_R = 0.2$. In contrast, $g_R = Z/A$ seems favorable in the $\pi h_{11/2}$ cases in Ref. 29. An explanation of the difference between experimental and calculated values of g_R was given by Bohr and Mottleson[33] as a blocking effect of the odd quasiparticle on the pairing gap. Furthermore, at least a part of this effect was shown to be taken into account by the coupling with gamma vibration[30] even if the calculated g_{RPA} is used in the mean-field step.

Electric quadrupole transition rates bring complementary information to energy spectra and $M1$ transitions, i.e., the information about the collective properties of nuclei. Calculated transition quadrupole moments Q_t ($\Delta J = 1,2$), which are proportional to the square roots of $B(E2;\ \Delta J = 1,2)$ respectively, are shown in Fig. 8(a). They were calculated using cranking wave functions without any *a priori* relation between the shapes and the quadrupole moments. They depend on ω very smoothly and reproduce the average of the experimental values well.

In summary of this subsection, an axially symmetric Nilsson plus BCS field with $\beta^{(\text{pot})} = 0.26$ ($\beta^{(\text{den})} \simeq 0.31$) has been proved to reproduce all the measured quantities very well.

B. [422 $\frac{5}{2}$] 3-qp band

Taking the pairing force strengths determined at the ground state, BCS calculations were performed at $\hbar\omega = 0.5$ MeV for some shapes with and without axial symmetry. Then, using calculated pairing gaps, energy spectra were calculated for each shape. It was found that not only $\gamma > 0$, but also $\beta(3\text{ qp}) > \beta(1\text{ qp})$ was necessary in order to reproduce the reduced signature splitting quantitatively. Although this shape differs from the prediction of the Woods-Saxon potential calculation,[4] it looks consistent with the stabilization of the moments of inertia after the band crossing. Calculated Q_t ($\Delta J = 1,2$) values using $\beta^{(\text{pot})} = 0.29$ and $\gamma^{(\text{pot})} = 20°$ ($\beta^{(\text{den})} \simeq 0.33$ and $\gamma^{(\text{den})} \simeq 12°$) are nearly the same as those of the 1-qp band [Fig. 8(a)], and the experimental Q_t ($\frac{33}{2} \rightarrow \frac{29}{2}$), which is the only data point belonging to the 3-qp band, is reproduced very well. Weak signature dependence appears in the calculated Q_t ($\Delta J = 1$) values as a result of the positive gamma deformation.

In the calculation of $B(M1)$,

$$g_{2\text{-qp}} = g_R + (g_p - g_R)\frac{i_{2p}}{I - i_n} \tag{4}$$

was used[34] in place of g_R in Eq. (1) so as to keep theoretical consistency with the use of $g_R = 0.3$ in the 1-qp band, although the g factor of the s-band configuration could be calculated microscopically. Here g_p is the g factor of quasiprotons; the Schmidt value calculated by using

TABLE VI. Parameters used in the theoretical calculation.

	$\beta^{(\text{pot})}$ $\beta^{(\text{den})}$	$\gamma^{(\text{pot})}$ $\gamma^{(\text{den})}$	Δ_n (MeV)	Δ_p (MeV)	λ_n ($\hbar\omega_0$)	λ_p ($\hbar\omega_0$)	g_R	g_p	i_n	i_{2p}
[422 $\frac{5}{2}$] 1 qp	0.26	0	1.30	1.30	4.96	4.76	0.30		2.0	
	0.31	0								
[422 $\frac{5}{2}$] 3 qp	0.29	20°	0.72	0.71	4.97	4.75	0.30	1.35	2.0	4.5
	0.33	12°								
[301 $\frac{3}{2}$] 1 qp	0.26	0	1.30	1.30	4.96	4.76	0.47		1.0	
	0.31	0								

[a] $\hbar\omega_0 = 41A^{-1/3}$ MeV.

$g_s^{(\text{eff})}=0.75g_s^{(\text{free})}$ was adopted. In the derivation of Eq. (4),

$$I=I_0+i_n=R+i_{2p}+i_n \tag{5}$$

is assumed. Since (g_p-g_R) in Eq. (4) is positive, the enhancement of $B(M1)$ due to the alignment can be predicted without introducing Dönau's semiclassical vector coupling.[9] The result is shown in Fig. 8(b). The calculated enhancement of $B(M1;\frac{33}{2}\rightarrow\frac{31}{2})$ appears somewhat small, but this is just a matter of parameter tuning.

In summary of this subsection, $\beta(3\text{ qp})>\beta(1\text{ qp})$ does not contradict available experimental information.

C. [301 $\frac{3}{2}$] 1-qp band

The calculation was performed using the same mean-field parameters as those for the [422 $\frac{5}{2}$] 1-qp band; therefore, the transition quadrupole moments shown in Figs. 8(a) and 10(a) are essentially the same except for the fact that i_n in Eq. (2) is different. The calculated $\Delta e'$ is shown in Fig. 10(c). Its sign is correct except for the lowest-frequency region, but the magnitude is somewhat smaller than the data.

We calculated the $B(M1)$ values using $g_R=Z/A$ since the blocking effect of natural parity orbitals on pairing gaps is weak. An example of the configuration dependence of g_R that reproduces the data of ^{161}Dy phenomenologically can be found in Tables 5-14 of Ref. 33. The result of our calculation is shown in Fig. 10(b). The ω dependence of the signature-averaged magnitude is reproduced, although the absolute magnitudes are smaller than the data. They are sensitive to β (and γ), i.e., the j mixing. The calculated signature dependence of $B(M1)$ is stronger than the data, although its phase agrees with the experimental one in the high-spin region. The relation between the signature splitting of the quasiparticle energy and the signature dependence of $B(M1)$ in natural parity bands was discussed in Ref. 10. According to it, the well-known phase rule for unique parity bands does not hold in general. The calculated phase relation is normal except for the lowest-frequency region in the present case.

The agreement between data and calculation is not as good as in the case of the $N=4$ intruder orbital. It may indicate that there is room to improve the potential parameters for small N shells.

VI. CONCLUSIONS

The lowest positive- and negative-parity rotational bands in ^{77}Kr have been studied following their production in the ^{48}Ti(^{32}S,2pn) reaction. The bands were extended up to spins of $(\frac{27}{2}^-)$ and $\frac{45}{2}^+$, and spins were assigned or confirmed based on directional correlation ratios. The mean lifetimes of 21 states were measured using the Doppler-shift attenuation method.

A cranking model analysis shows a considerable similarity among the odd krypton isotopes ^{75,77,79}Kr. All of them show a quasiparticle alignment in the range 0.50 MeV $\leq\hbar\omega\leq$0.65 MeV. The sharpness of the $\pi g_{9/2}$ alignment in the $\pi=+$ band of ^{77}Kr is signature dependent. The possible beginning of a second, probably $\nu g_{9/2}$, alignment is seen at $\hbar\omega\approx$0.9 MeV. The kinematic and dynamic moments of inertia converge to a common value of (22–24)$\hbar^2$/MeV, perhaps indicating the onset of rigid rotation. The transition quadrupole moments in the positive-parity band of ^{77}Kr imply a rather strong deformation of $\beta_2\approx$0.33.

In the negative-parity band of ^{77}Kr, the beginning of an alignment can be seen at $\hbar\omega$=0.55 MeV in the $\alpha=+\frac{1}{2}$ signature, while there is no sign of irregularity up to 0.65 MeV in the $\alpha=-\frac{1}{2}$ signature. This is very similar to the behavior in ^{75}Kr except that the signatures are reversed. There is a steady increase in the moment of inertia with increasing rotational frequency in both nuclei at the same time that the transition quadrupole moments in ^{77}Kr decrease. It would be interesting to see if the trend persists in ^{75}Kr when lifetimes are measured for that nucleus.

The large number of $\Delta J=1$ transitions seen in ^{77}Kr from states of known lifetimes allows a better investigation of the pattern of $B(M1)$ strengths. A strong signature-dependent alternation of $B(M1)$ values is seen in the positive-parity band, but not in the negative-parity band, which shows little signature splitting. In the positive-parity band, the $M1$ strengths increase to the order of one single-particle unit after the $\pi g_{9/2}$ alignment.

Cranked Nilsson plus BCS calculations with $\beta^{(\text{pot})}=0.26$ ($\beta^{(\text{den})}\simeq0.31$) reproduce all the observed properties of the positive-parity 1-qp band excellently. Not only $\gamma>0$ but also $\beta(3\text{ qp})>\beta(1\text{ qp})$ have been shown to be necessary to reproduce quantitatively the reduced signature splitting after the band crossing. The agreement between data and calculation is not as good for the negative-parity band.

ACKNOWLEDGMENTS

This work was supported in part by the National Science Foundation and in part by the Grant-in-Aid for Scientific Research from the Ministry of Education, Science and Culture (No. 01790182). One of the authors (M.M.) is indebted to Fellowships of the Japan Society for the Promotion of Science for Japanese Junior Scientists. Two of the authors (S.G.B.) and (F.E.D.) acknowledge support through the Louisiana Board of Regents EPSCoR Program, Grant No. NSF/LaSER (1989)-RFAP-05.

[1]S. L. Tabor, P. D. Cottle, J. W. Holcomb, T. D. Johnson, P. C. Womble, S. G. Buccino, and F. E. Durham, Phys. Rev. C **41**. 2658 (1990).

[2]B. J. Varley, M. Campbell, A. A. Chisti, W. Gelletly, L. Goettig, C. J. Lister, A. N. James, and O. Skeppstedt, Phys. Lett. B **194**, 463 (1987).

[3]R. B. Piercey, J. H. Hamilton, R. Soundranoyagam, A. V. Ramayya, C. F. Maguire, X.-J. Sun, Z. Z. Zao, R. L. Robin-

son, H. J. Kim, S. Frauendorf, J. Döring, L. Funke, G. Winter, J. Roth, L. Cleeman, J. Eberth, W. Neumann, J. C. Wells, J. Lin, A. C. Rester, and H. K. Carter, Phys. Rev. Lett. **47**, 1514 (1981).

[4]C. J. Gross, P. D. Cottle, D. M. Headly, U. J. Hüttmeier, E. F. Moore, and S. L. Tabor, Phys. Rev. C **36**, 2601 (1987).

[5]C. J. Gross, J. Heese, K. P. Lieb, S. Ulbig, W. Nazarewicz, C. J. Lister, B. J. Varley, J. Billowes, A. A. Chishti, J. H. McNeil, and W. Gelletly, Nucl. Phys. **A501**, 367 (1989).

[6]M. S. Kaplan, J. X. Saladin, L. Faro, D. F. Winchell, H. Takai, and C. N. Knott, Phys. Lett. B **215**, 251 (1988).

[7]I. Hamamoto and H. Sagawa, Nucl. Phys. **A327**, 99 (1979).

[8]Ikuko Hamamoto, Phys. Lett. **106B**, 281 (1981).

[9]F. Dönau, Nucl. Phys. **A471**, 469 (1987).

[10]Masayuki Matsuzaki, Phys. Rev. C **39**, 691 (1989).

[11]E. Nolte and P. Vogt, Z. Phys. A **275**, 33 (1975).

[12]B. Wörmann, K. P. Lieb, R. Diller, L. Lühmann, J. Keinonen, L. Cleeman, and J. Eberth, Nucl. Phys. **A431**, 170 (1984).

[13]F. Dönau, Niels Bohr Institute report, 1985.

[14]E. F. Moore, P. C. Cottle, C. J. Gross, D. M. Headly, U. J. Hüttmeier, S. L. Tabor, and W. Nazarewicz, Phys. Rev. C **38**, 696 (1988).

[15]L. C. Northcliffe and R. F. Schilling, Nucl. Data Sect. A **7**, 233 (1970).

[16]S. Kalbitzer, H. Oetzmann, N. Graham, and A. Feverstein, Z. Phys. A **278**, 223 (1976).

[17]J. Lindhard, M. Scharff, and H. E. Schiott, Mat. Fys. Medd. Dan. Vid. Selsk. **33**, No. 14 (1963).

[18]A. E. Blaugrund, Nucl. Phys. **88**, 501 (1966).

[19]H. P. Hellmeister, J. Keinonen, K. P. Lieb, U. Kaup, R. Rasher, R. Ballini, J. Delavnay, and H. Dumont, Nucl. Phys. **A332**, 241 (1979).

[20]F. Cristancho and K. P. Lieb, Nucl. Phys. **A456**, 353 (1988).

[21]A. A. Chisti, W. Gelletly, C. J. Lister, J. H. McNeill, B. J. Varley, D. J. G. Love, and O. Skeppstedt, Nucl. Phys. **A501**, 568 (1989).

[22]D. F. Winchell, M. S. Kaplan, J. X. Saladin, H. Takai, J. J. Kolata, and J. Dudek, Phys. Rev. C **40**, 2672 (1989).

[23]G. Winter, J. Döring, L. Funke, H. Prade, H. Rotter, R. Schwengner, A. Johnson, and A. Nilsson, J. Phys. G **14**, L13 (1988); R. Schwengner, J. Döring, L. Funke, G. Winter, A. Johnson, and W. Nazarewicz, Nucl. Phys. **A509**, 550 (1990).

[24]H. G. Price, C. J. Lister, B. J. Varley, W. Gelletly, and J. W. Olness, Phys. Rev. Lett. **51**, 1842 (1983).

[25]S. L. Tabor, Phys. Rev. C **34**, 311 (1986).

[26]L. Funke, F. Dönau, J. Döring, P. Kemnitz, E. Will, G. Winter, L. Hildingsson, A. Johnson, and Th. Lindblad, Phys. Lett. **120B**, 301 (1983); L. Funke, J. Döring, P. Kemnitz, E. Will, G. Winter, A. Johnson, L. Hildingsson, and Th. Lindblad, Nucl. Phys. **A455**, 206 (1986).

[27]P. Kemnitz, J. Döring, L. Funke, G. Winter, L. H. Hildingsson, D. Jerrestam, A. Johnson, and Th. Lindblad, Nucl. Phys. **A456**, 89 (1986).

[28]J. D. Garrett, J. Nyberg, C. H. Yu, J. M. Espino, and M. J. Godfrey, in *International Conference on Contemporary Topics in Nuclear Structure Physics,* edited by R. Casten, A. Frank, M. Moshinsky, and S. Pittel (World Scientific, Singapore, 1988), p. 699.

[29]M. Matsuzaki, Y. R. Shimizu, and K. Matsuyanagi, Prog. Theor. Phys. **79**, 836 (1988).

[30]M. Oshima, M. Matsuzaki, S. Ichikawa, H. Iimura, H. Kusakari, T. Inamura, A. Hashizume, and M. Sugawara, Phys. Rev. C **40**, 2084 (1989).

[31]Y. R. Shimizu and K. Matsuyanagi, Prog. Theor. Phys. **74**, 1346 (1985).

[32]The definitions of $(\beta^{(\mathrm{pot})},\gamma^{(\mathrm{pot})})$ and $(\beta^{(\mathrm{den})},\gamma^{(\mathrm{den})})$ were given in Appendix B of Y. R. Shimizu and K. Matsuyanagi, Prog. Theor. Phys. **71**, 960 (1984). Note that the sign of γ was defined oppositely to the Lund convention in this reference.

[33]A. Bohr and B. R. Mottelson, *Nuclear Structure* (Benjamin, Reading, MA, 1975), Vol. II.

[34]S. Frauendorf, Phys. Lett. **100B**, 219 (1981).